

# Performance parameters for evaluating the pore detection ability of computed tomography systems

Katja Höger<sup>1</sup>, Leonard Schild<sup>1</sup>, Lukas Weiser<sup>1</sup>, Gisela Lanza<sup>1</sup>

<sup>1</sup>wbk Institute of Production Science, Karlsruhe Institute of Technology (KIT), Karlsruhe, Germany, e-mail: katja.hoeger@kit.edu

## Abstract

Industrial x-ray computed tomography (CT) has become an important tool for detecting and characterizing pores in workpieces produced through additive manufacturing (AM). However, a procedure to quantify the ability of a CT system to reliably detect pores, ideally in a non-destructive manner and before the actual analysis process, is still being researched. Previous approaches can either only be carried out at a great expense and destructively, or have not yet been validated in the actual case of pore detection. This work presents a potential reference object and corresponding performance parameters, the metrological structural resolution and the grey-scale resolution. To investigate their suitability for predicting the ability to detect pores, both the reference object, and special pore-containing AM samples were examined using the same CT settings. Linking the performance parameters with the pore detection rate of the AM samples showed that structural resolution, but also image sharpness, are suitable parameters.

**Keywords:** Computed Tomography, Pore Detection, Additive Manufacturing, Resolution

## 1 Introduction

Industrial x-ray computed tomography (CT) has become an important tool for detecting and characterising pores in workpieces [1]. The main reason is CT's ability to examine internal structures non-destructively and in three dimensions. An important area of application is the additive manufacturing (AM), as it cannot yet avoid internal defects with negative effects on mechanical properties [2,3]. However, because CT technology is a relatively new measurement technique, its capabilities, such as accuracy and reliability, are not always precisely known, particularly in industrial applications.

Possible approaches to evaluate CT's ability to accurately analyse pores are to either compare CT to a higher resolution measurement technique, deploy reference objects with artificial pores, or use performance parameters such as the image resolution.

Regarding the first approach, the most widely used method compares micrographs of cross-sections with the CT scan, cf. e.g. [3–6]. Therein, the major challenge lies in the precise alignment of the real and virtual cross-sections [5]. One promising method involves scanning the workpiece before and after the cutting process, then aligning both scans to identify the exact location of the cross-section in the uncut volume's reconstruction [3]. The advantage of this approach is that real pores are examined, as they result from the AM process. However, preparing the micrographs is time-consuming and involves destroying the workpiece.

The second approach, proposed in [1], uses a specially designed object that contains small, hemispherical holes in the size of typical pores of the AM process. The object allows tactile calibration of the holes before CT measurements, which serves as a reference for the CT results. This approach proved to be appropriate for identifying suitable CT scanning and pore detection parameters for the reference object and the actual AM specimens. Nevertheless, the transferability of the behaviour of these artificial pores to actual pores is still being investigated.

The third approach is to use respective CT performance indicators. Literature proposes certain indicators like the maximum permissible error for typical metrological tasks [7]. Indicators that quantify resolution seem similarly suitable to represent defect analysis, such as pore detection. Resolution is a measure of the minimum size up to which structures can be separately resolved [7]. In principle, this allows a statement about the ability to dissolve pores. Various parameters, as well as determination procedures, have been presented to quantify resolution [7,8]. Resolution on the grey scale level can be specified using the modulation transfer function (MTF), the spatial frequency response, and measured via a cylinder following ASTM E1695:20 [9]. Resolution in dimensional measurements can be specified using the measurement structural resolution (MSR) or the interface structural resolution (ISR) [8,10]. MSR refers to the resolution behaviour on a single (curved) external surface element. ISR, on the other hand, assesses the ability to resolve two closely converging surfaces. Its value describes the resolvable distance between these inner surfaces. [10] For determining the ability to detect pores (inner structures) in a volume, ISR seems more advantageous than MSR. A possible method of its assessment is the "two-spheres standard", introduced in [10,11]. It is based on evaluating the contact zone of two spheres with known radii. By measuring the height at different distances from the contact zone and comparing it to the reference height, the smallest distance measurable within an error limit can be determined. The transferability of the discussed resolution parameters to actual defect analysis results has yet to be investigated, though.

To summarize, the above-mentioned reference objects and performance parameters have yet to be evaluated in terms of their capability to reliably, non-destructively and rapidly quantify a CT system's ability to detect pores in AM components. To address



this gap, this work proposes two related test objects and a corresponding procedure, cf. Figure 1. The first test object is a reference object to assess resolution using the performance parameters ISR and MTF. The second test object is made by AM and therefore naturally contains pores. By first preparing CT scans and micrographs of cross-sections of the second test object, the actual pore resolution can be determined. By scanning both test objects with the same CT system and settings, transferability of ISR and MTF to the actual pore resolution is investigated.

The test objects are presented in Section 2. Subsequently, Section 3 describes results from the procedure to investigate the applicability of the proposed test objects and performance parameters to predict actual pore resolution. Finally, a conclusion is drawn in Section 4.

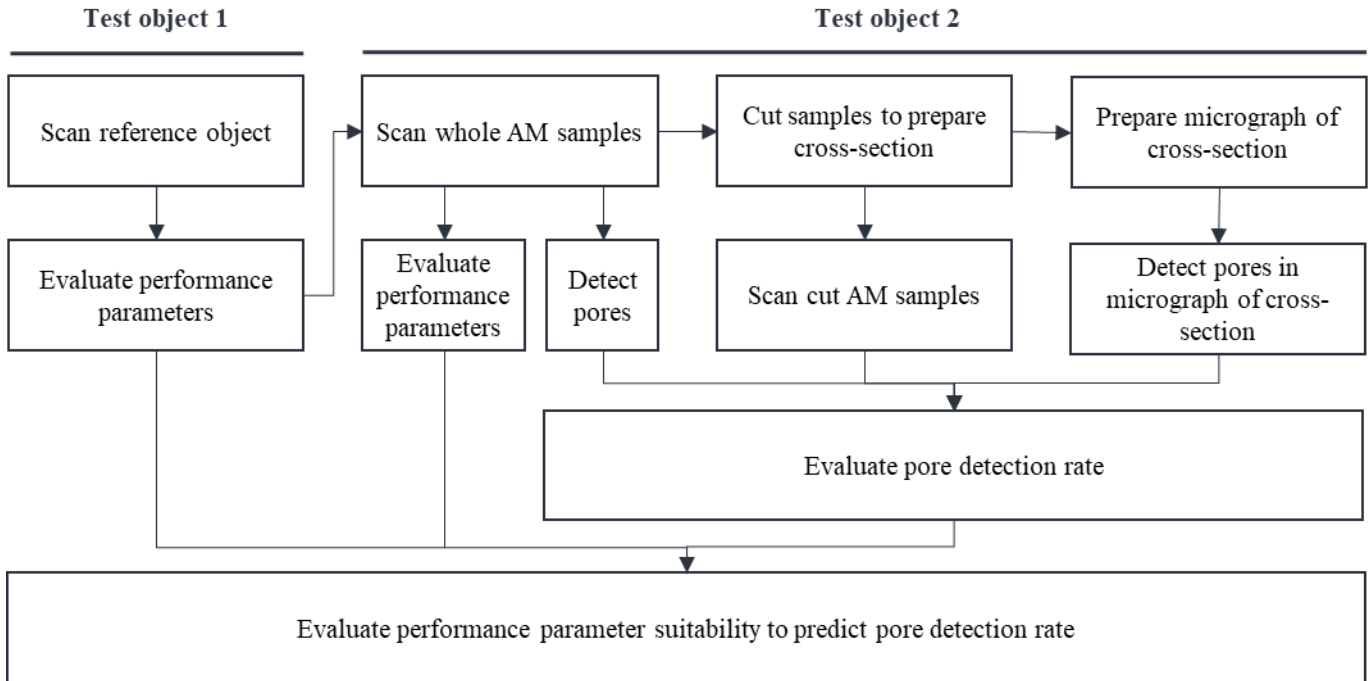


Figure 1: Procedure for investigating the suitability of the test object, MSR and ISR to predict pore detection rate.

## 2 Test objects and their parameters for resolution assessment

### 2.1 Test object 1 and performance parameters

Figure 2 shows the proposed reference object (test object 1). The reference object consists of a hull that contains two spheres in a rotationally symmetrical hole. The spheres were acquired from a specialized supplier. The hull was produced by means of milling. High-precision manufacturing ensured perfect alignment of the spheres. The object can be easily scaled and made from different materials, thereby enabling adaptation to different applications. However, the manufacturing process is complex. The spheres must be inserted both without tolerance and pressure to prevent displacement during the CT scan and mechanical widening of the contact point, respectively.

This work examines reference objects made of 316L stainless steel (1.4404) with a height of 10 mm and a maximum diameter of 5 mm. The dimensions were adapted according to the power of the X-ray source of the used CT system, a Metrotom 800 (130kV) device from Zeiss IMT GmbH (Germany).

By analysing the spheres' touching point, the ISR can be determined according to the two-spheres method [11] (cf. Section 2.1.1). Following the ASTM E1695:20 standard [9], the MTF can be determined via the cylindrical outer contour (cf. Section 2.1.2). To enable equal component alignment for analysis, a small hole in the cylinder's outer surface is provided.

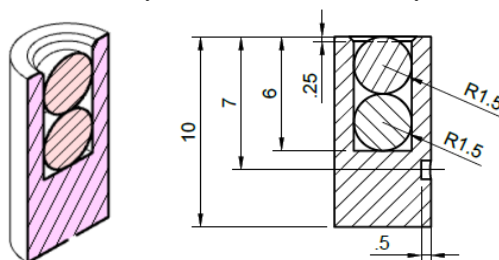


Figure 2: Cut view (left) and technical drawing (right) of CT setting Cu50\_80\_1 (right) of the reference object.

### 2.1.1 ISR

Resolution in dimensional measurements is specified via the ISR, which is determined by applying the two-spheres method [11]. This method evaluates the error  $\Delta$  between a measurement  $h_m$  evaluated in the CT reconstruction, and the corresponding reference value  $h_r$  (cf. Figure 3). In this work, an error limit of 10 % is used, which means that ISR equals the smallest  $h_m$  that lead to a  $\Delta$  smaller than 10 %:

$$\text{ISR} = \text{ISR}_{10} = h_{m,i} \in h_m \min\{\Delta_i < 10\% \} \text{ with } \Delta_i = \frac{\text{abs}(h_{r,i} - h_{m,i})}{h_{r,i}} \quad (1)$$

For its determination, circles are fitted at different distances  $i$  to the contact point of the spheres (in the direction of the line through the spheres' centres) using VGStudio Max 3.4 software. Based on the radii of these circles ( $r_{m1,i}$ ,  $r_{m2,i}$ ), as well as the sphere diameters ( $R_1$ ,  $R_2$ ) and the distance between the sphere centres ( $\overline{C_1C_2}$ ), the heights can be deduced:

$$h_{m,i} = 2i \quad \text{and} \quad h_{r,i} = \overline{C_1C_2} - \sqrt{R_1^2 - r_{m1,i}^2} - \sqrt{R_2^2 - r_{m2,i}^2} \quad (2)$$

In contrast to [11],  $\overline{C_1C_2}$  (instead of  $R_1 + R_2$ ) is used for calculation, as the sphere's contact is not a perfect point, but a touching area. Despite the high-precision manufacturing, this widening appeared.

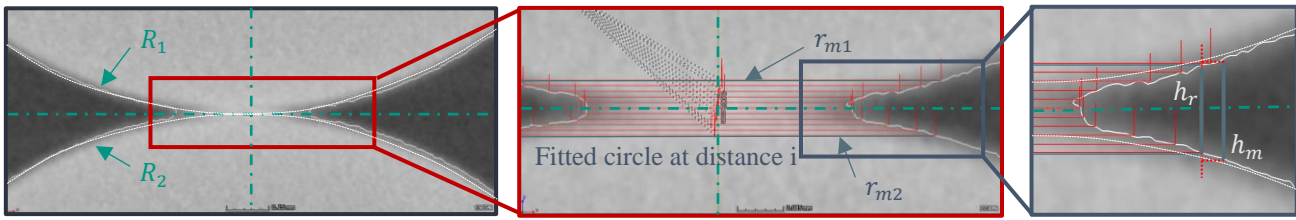


Figure 3: Determination of the heights  $h_m$  and  $h_r$  after [11].

### 2.1.2 Resolution parameter $f_{10}$ deduced from MTF

Resolution in the grey scale range is defined via the frequency  $f_{10}$  at 10 % of the MTF. This resolution parameter allows a prognosis of the detection limit of a structure in volume image data [7,12]. MTF is determined via the cylindrical outer contour. The standard ASTM E1695-20 [9] normally requires MTF's determination on three planes that intersect the object perpendicular to the axis of rotation at the object's centre and 15 % from its top and bottom. To obtain complete circles in the sectional view of the present object, only the volume from the bottom of the object to the small outer hole is used (cf. Figure 4). All section planes are defined perpendicular to the cylinder axis but evaluated in the unaligned volume. The remaining measurement parameters (bin size, number of fit points) are determined following the ASTM standard. Figure 5 depicts an exemplary section plane (CT setting CU50\_25\_1) and its corresponding MTF.

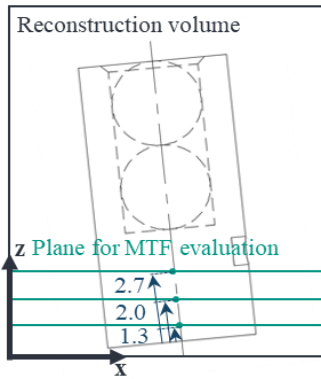


Figure 4: Planes used for MTF evaluation.

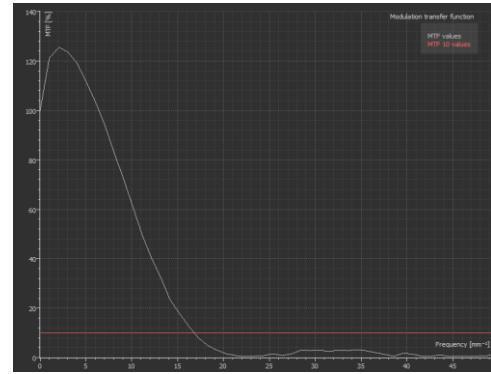
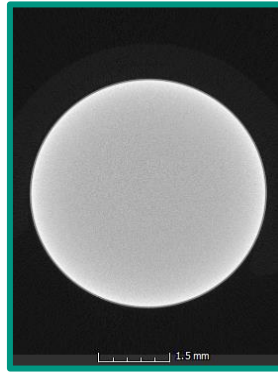


Figure 5: Exemplary section plane and corresponding MTF.

### 2.1.3 Image Quality

In addition to ISR and MSR, image quality parameters were evaluated using Matlab 2021a (MathWorks Inc.) software for calculations. For quantifying global image quality, the histogram-based contrast-to-noise ratio (CNR) was used. It was assessed via the grey-value distributions of the histograms of the reconstruction and calculated using the method presented in [13]. Contrast is determined based on the grey values of the peaks of the background  $G_{B,\max}$ , and material  $G_{M,\max}$  in the smoothed histogram (smoothing applied with a moving average filter with a window size of 1/50 of histogram bin locations), cf. Figure 6. Image noise relates to the area  $\Delta G_1$  that encompasses 95% of the voxels located between the left edge and the left peak, i.e. voxels in the background. [13] The calculation was carried out to the following equation:

$$\text{CNR} = \frac{G_{M,\max} - G_{B,\max}}{\Delta G_1} \quad (3)$$

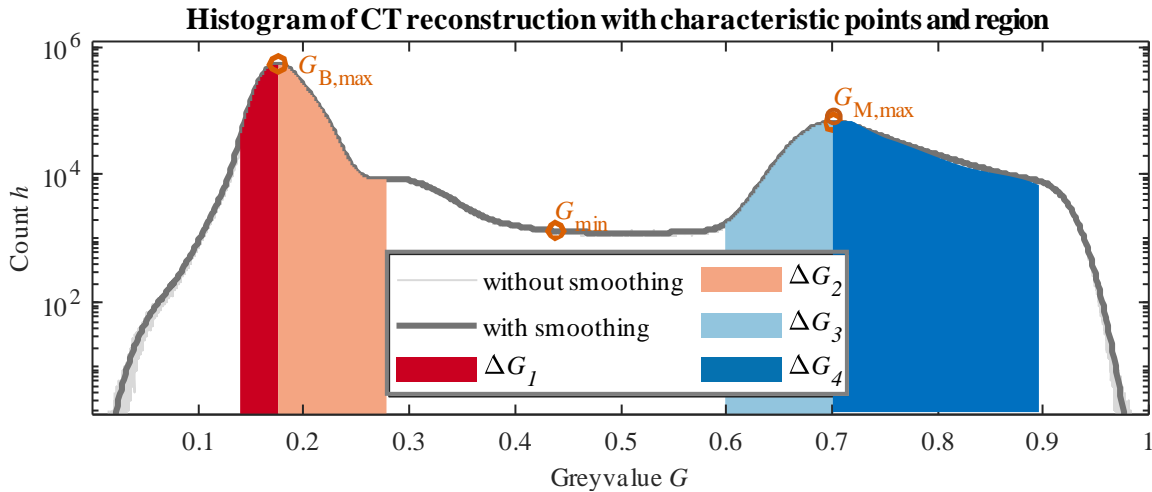


Figure 6: Histogram of a CT reconstruction including characteristic points and regions for the calculation of the image quality parameter CNR.

Besides CNR, image sharpness  $S$  was determined as a generalization of the MTF assessment method [14] (cf. Section 4.3.2 and 4.3.3). Equivalent to the MTF determination, the section planes of the reconstruction were used. In these section planes all edges were detected (using edge detection filter canny and Matlab function *edge*), then divided into segments of 42-pixel length. For each segment, vertically aligned vectors with a total length of 81 pixels (intersection pixel plus 40 pixels in each direction) were determined. Figure 7 (left) depicts a resulting example section plane, including segments and corresponding vectors.

Next, local sharpness  $s$  was calculated at each vector intersection. In this work, local sharpness  $s$  is defined as the largest grey value difference (largest slope  $\delta(G)_{max}$ ) within 1 pixel of the intersection and is referenced to the local contrast, as proposed from Schild [14]. Therein, local contrast describes the difference between the mean material grey values  $\bar{G}_M$  and the mean background grey values  $\bar{G}_B$ . Figure 7 (right) shows an exemplary grey value profile of the vector on edge 31, including the features for local sharpness evaluation. The mean value of all scaled local sharpness values from all segments is defined as sharpness  $S$ :

$$S = \frac{1}{n} \sum_{i=1}^n s_i \text{ with } s_i = \frac{\delta(G_i)_{max}}{\bar{G}_{Mi} - \bar{G}_{Bi}} \quad (4)$$

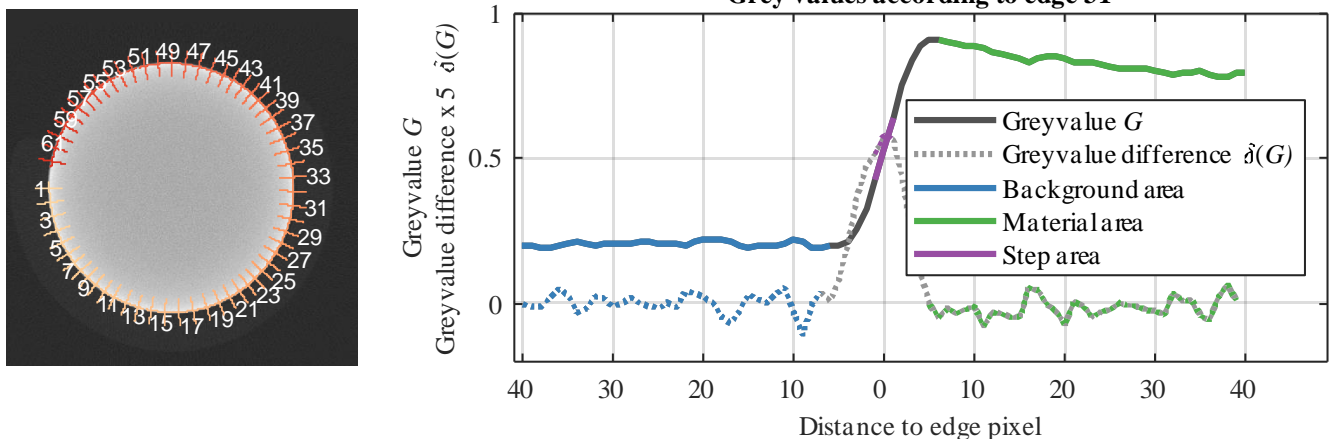


Figure 7: Exemplary section plane including edge segments and vectors (left) and corresponding grey value profile of edge 31 (right).

## 2.2 Test object 2 and pore detection rate

As test object 2, AM samples were manufactured using powder bed fusion – laser beam/metal (PBF-LB/M). Due to this process, these samples naturally contained pores. Five samples were manufactured. Figure 8 illustrates an exemplary AM sample. To allow a comparison to test object 1 external dimensions and material are the same.

The ability to detect pores was quantified by the pore detection rate (cf. Section 3.2). For assessing the pore detection rate, pores detected in micrographs of cross-sections were compared with the corresponding pores detected in an equivalent section of the CT scan (VGStudio’s VGEasyPore algorithm was used for pore detection). Figure 9 shows an exemplary comparison of the micrograph image of a cross-section and the corresponding cross-section in the CT reconstruction.

To evaluate the same cross-section in the CT reconstruction as in the micrograph, the samples’ special design was used. Only the cylindrical part of the sample is used for pore analysis. The features located in the upper half of the sample serve to define a local coordinate system, allowing accurate sample alignment in the CT reconstruction. Using the thread, a nut can be screwed

on to protect the registration features during the preparation of the cross-section. By scanning the sample before and after cutting and aligning both scans, the cross-sections can be identified in the reconstruction of the cut sample and transferred to the reconstruction of the uncut sample.



Figure 8: Photo of AM sample.

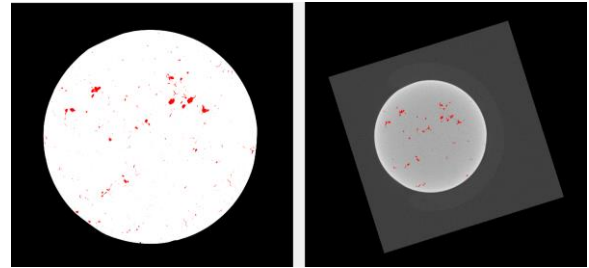


Figure 9: Comparison of a micrograph image of a cross-section (left) and a CT image of the same cross-section (right).

### 3 Experimental results and evaluation

For comparing performance parameters and actual pore resolution (via the pore detection rate), both must be investigated using same conditions. CT settings were defined by scanning and analysing the behaviour of the reference object at different CT settings (Section 3.1). Then, the five AM samples were scanned using these settings, and the respective pore detection rate was determined (Section 3.2). Moreover,  $f_{10}$  and image quality parameters were evaluated using the same approach as for the reference object. Finally, the results from the reference object and the AM samples were compared (Section 3.3).

#### 3.1 Definition of CT settings and evaluation of performance parameter behaviour

CT settings were defined in a two-step approach. First, a variety of different CT settings were defined and tested with the reference object (test object 1). Next, the CT settings were narrowed down to the most interesting ("extreme") CT settings to limit the further experimental scope.

The initial selection of CT settings was done using the method according to Schild [14]. This method defines experimental points at the edge of the linear detector range. Thus, the maximum possible variance between settings is achieved, which results in varying image quality, and hence resolution. Accordingly, current and voltage of the x-ray tube were varied for four combinations of pre-filter thickness (copper filter) and detector gain [14]. The remaining CT parameters were held constant (1450 projections with an exposure time of 1000 ms, no binning, 360° rotation). This resulted in 16 different settings (cf. Table 1). For each of the CT settings, the performance parameters ISR and  $f_{10}$  and the image quality of the reconstruction were evaluated. For setting CU100\_80\_1, additional 5 repeat measurements were carried out to obtain an estimate of the standard deviation of the experiment.

Table 1: CT settings used for investigating the reference object.

Name	Filter (10 μm)	Gain (-)	CT Setting	Voltage (kV)	Current (μA)	Power (W)
<b>CU50_25_1</b>	<b>50</b>	<b>2.5</b>	<b>1</b>	<b>130</b>	<b>300</b>	<b>39</b>
CU50_25_3	50	2.5	3	130	220	29
CU50_25_4	50	2.5	4	120	300	36
CU50_25_5	50	2.5	5	127	280	36
<b>CU50_80_1</b>	<b>50</b>	<b>8.0</b>	<b>1</b>	<b>130</b>	<b>93</b>	<b>12</b>
CU50_80_2	50	8.0	2	88	300	26
CU50_80_4	50	8.0	4	103	300	31
CU50_80_5	50	8.0	5	113	197	22
<b>CU100_25_1</b>	<b>100</b>	<b>2.5</b>	<b>1</b>	<b>130</b>	<b>300</b>	<b>39</b>
CU100_25_3	100	2.5	3	130	280	36
CU100_25_4	100	2.5	4	127	300	38
<b>CU100_80_1</b>	<b>100</b>	<b>8.0</b>	<b>1</b>	<b>130</b>	<b>165</b>	<b>21</b>
CU100_80_2	100	8.0	2	108	300	32
CU100_80_3	100	8.0	3	130	125	16
CU100_80_4	100	8.0	4	110	300	33
CU100_80_5	100	8.0	5	120	223	27

Figure 10 shows the influence of different CT parameter setting combinations on the performance parameters ISR,  $f_{10}$  and CNR. The performance parameters were normalised to their respective largest values. While low ISR values indicate high resolution, high values for  $f_{10}$  and CNR represent high image quality. In addition, the figure shows the estimate of the standard deviation via the double confidence interval (assuming a t-distribution), based on the repeated measurements of the setting CU100\_80\_1. ISR values range between 1 and 0.61,  $f_{10}$  values between 1 and 0.78 and CNR values between 1 and 0.58.

The size and material of the reference object limited the possible CT settings within each filter-gain combination. Combinations using a gain of 2.5 resulted in similar voltage and current values at all experimental points. The same applied to settings 2 and 4 with a copper filter of 1000  $\mu\text{m}$  and a gain of 8.0 (cf. Table 1). These similarities were reproduced by the performance parameters. When comparing different filter-gain combinations (and thus CT settings), different performance parameter values were obtained. CT settings with a higher gain (8.0 compared to 2.5) enabled lower power of the x-ray source and thus resulted in a higher resolution (lower ISR). This was especially apparent for setting CU050\_80\_1, where the power could be reduced below 16 W. This enabled a focal spot size of  $\sim 20 \mu\text{m}$  compared to a spot size of  $\sim 40 \mu\text{m}$  for all other settings. On the other hand, increased gain led to more noise and thus a decreasing CNR value. Figure 11 shows exemplary projections for different CT setting combinations.

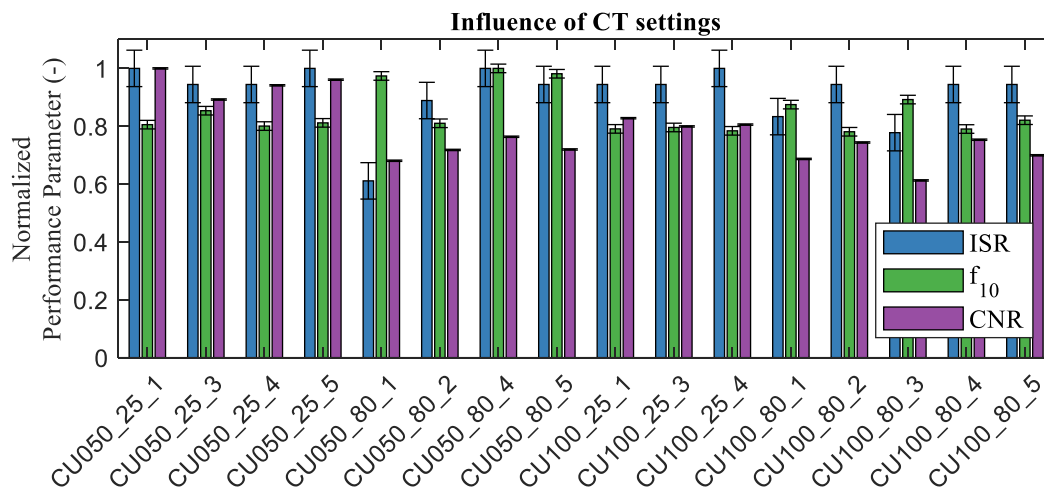


Figure 10: Influence of different CT setting combinations on the normalized performance parameters ISR,  $f_{10}$  and CNR.

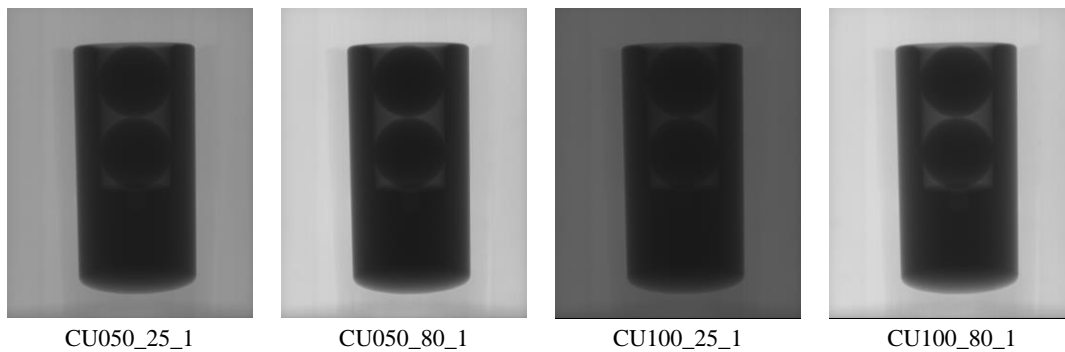


Figure 11: Projection of different CT setting combinations of the reference object.

For the following analysis only four exemplary “extreme” settings that resulted in considerably different performances were selected. This allows to draw a general conclusion regarding the method’s applicability while limiting experimental efforts. CT settings 1 for each filter-gain combination were chosen as extreme settings due to the following reasons:

- CU050\_25\_1: CT setting with highest image quality (high CNR)
- CU050\_80\_1: CT setting with the highest resolution (low ISR and high  $f_{10}$ )
- CU100\_25\_1: CT setting with balanced performance parameters at medium level and high image quality (high CNR)
- CU100\_80\_1: CT setting with balanced performance parameters at medium level and high resolution (low ISR)

The corresponding settings are marked in bold in Table 1. In the remaining work, these CT settings are indicated only by their filter-gain combination (e.g. CU050\_25 instead of CU050\_25\_1) to enhance readability.

### 3.2 Pore detection rate in AM samples

For each AM sample and each CT setting, the pore detection rate was determined by comparing the number of pores of a given area or larger found in the micrograph cross-section and the corresponding slice from a CT reconstruction representing the cross-section (cf. Section 2.2, Figure 9). Figure 12 shows the detection rate as a function of the pore area for all CT settings. Pore area was defined by the voxel size (voxel edge length of 7  $\mu\text{m}$ ).

Figure 12 indicates that certain minimum pore size is necessary to achieve high detection rates of over 60 %. CT settings leading to high sharpness and resolution (gain of 8.0) lead to higher pore detection rates for pores of similar size compared to settings with a high CNR but a low resolution (gain of 2.5).

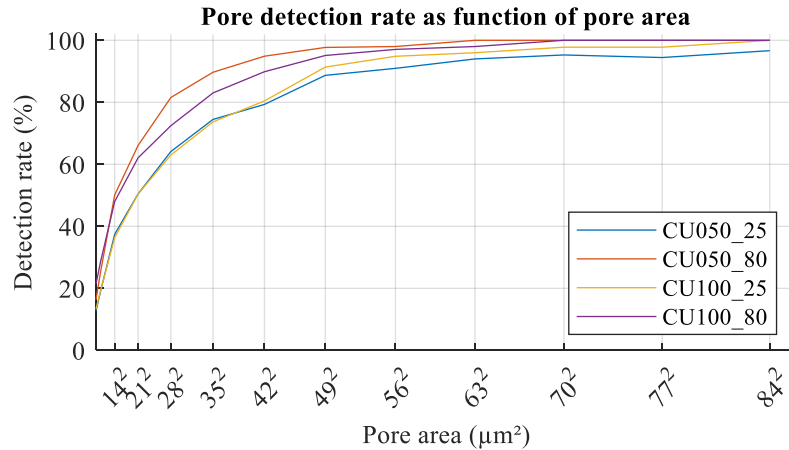


Figure 12: Pore detection rate achieved by using different CT settings. The pore detection rate is depicted as a function of the pore area.

### 3.3 Performance parameters and pore detection rate

The following section addresses the relationship between performance parameters and pore detection rate in more detail. For these evaluations, the results from test object 1 (ISR,  $f_{10}$ , image quality) were compared to the results from test object 2 (pore detection rate).

#### 3.3.1 ISR and pore detection rate

Figure 13 presents the ISR as a function of the pore detection rate for different minimal pore areas. For the representations, the detection rate at a specific minimal pore area was determined for each CT setting combination, and linked to the setting-related ISR. This comparison takes advantages of the fact that the test objects' dimensions and materials are similar.

The results show a linear relationship between ISR and pore detection rate (regression coefficients shown in the title). With increasing resolution (decreasing ISR), the pore detection rate increases. More explicitly, the ISR parameter indicates a pore detection rate of 67 % - 75 % of all pores having at least the area of the squared ISR value (compare dotted line in Figure 13 which corresponds to the pore area).

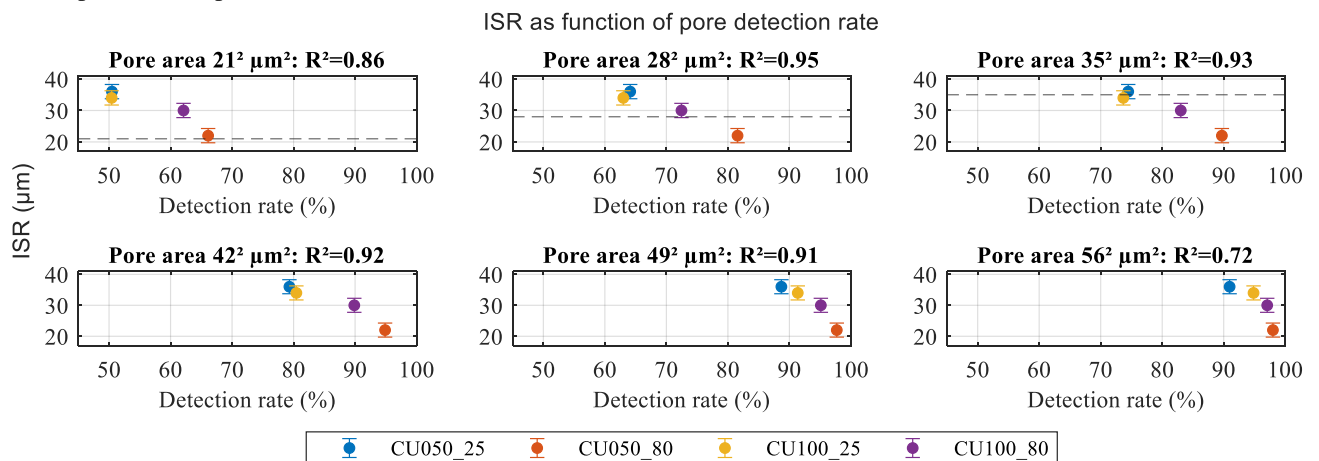


Figure 13: Influence of ISR on the pore detection rate for different minimal pore areas.

One explanation for not reaching 100 % when including small pore areas is the complexity of the task: Pore detection depends not only on pore area but also on other pore parameters, such as shape, as exemplified in Figure 14. A branched pore cannot be detected, as the individual branches are smaller than the resolution limit. Another explanation may be the dependency of ISR on a surface determination step. Pore analysis, on the other hand, is solely carried out on image data.

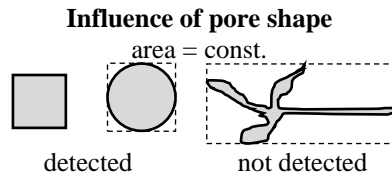


Figure 14: Possible pore shapes, all having the same pore area, and their influence on pore detection.

### 3.3.2 $f_{10}$ and pore detection rate

Figure 15 presents the pore detection rate related to the resolution at the grey scale level (i.e., based on the image data), represented via  $f_{10}$ , for different pore areas. For comparability with ISR, the reciprocal of  $f_{10}$  is used (lower values indicate higher resolution). The results show a linear relationship between  $f_{10}$  and pore detection rate. The  $f_{10}$  seems equally suitable for predicting the CT system’s ability to detect pores.

A more in-depth investigation of  $f_{10}$  however shows several disadvantages. According to the ASTM standard [9], inappropriate image data quality, resulting for example from excessive beam hardening or noise, disturbs  $f_{10}$  determination. Beam hardening leads to overshoots in the MTF, causing higher, but false,  $f_{10}$  values. Excessive noise influences the reproducibility of the value. All reconstruction slices show these beam hardening effects, cf. Figure 5. Moreover, it would be expected that the reference object and AM specimen show the same  $f_{10}$  values when using the same CT settings. As presented in Figure 17 a), this transferability is lacking.

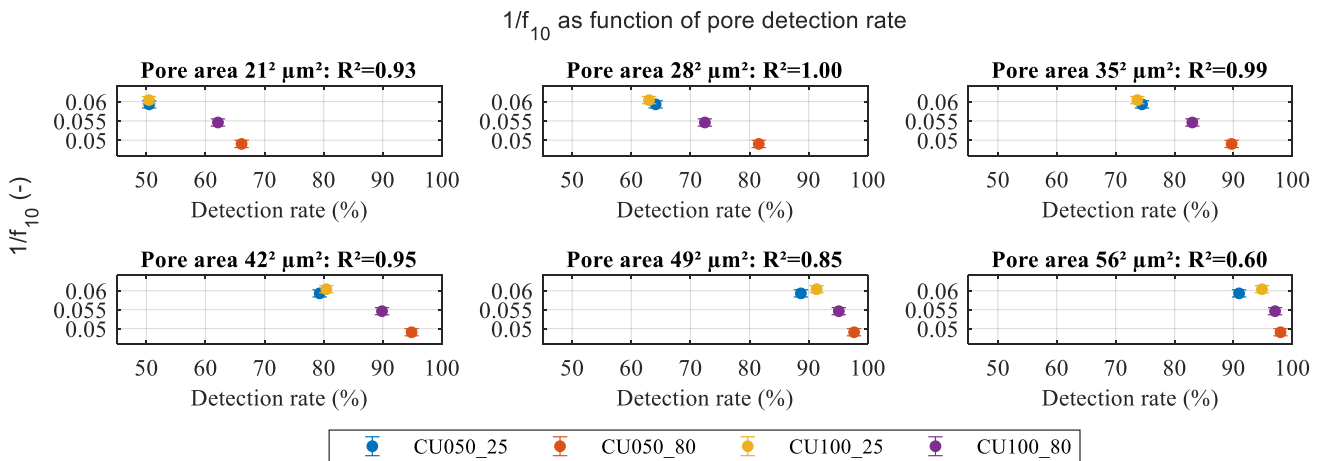


Figure 15: Influence of  $f_{10}$  on the pore detection rate for different minimal pore areas.

### 3.3.3 Image quality and pore detection rate

Figure 16 presents the pore detection rate related to the image sharpness  $S$  for different pore areas. As for  $f_{10}$  representation, the reciprocal is used. This parameter showed the same behaviour as the ISR and  $f_{10}$  parameters. Moreover,  $S$  values evaluated with the reference object and the AM samples are in good agreement, cf. Figure 17 b). Following, a parameter describing image quality via sharpness at the part edges seems suitable for predicting the pore detection ability.

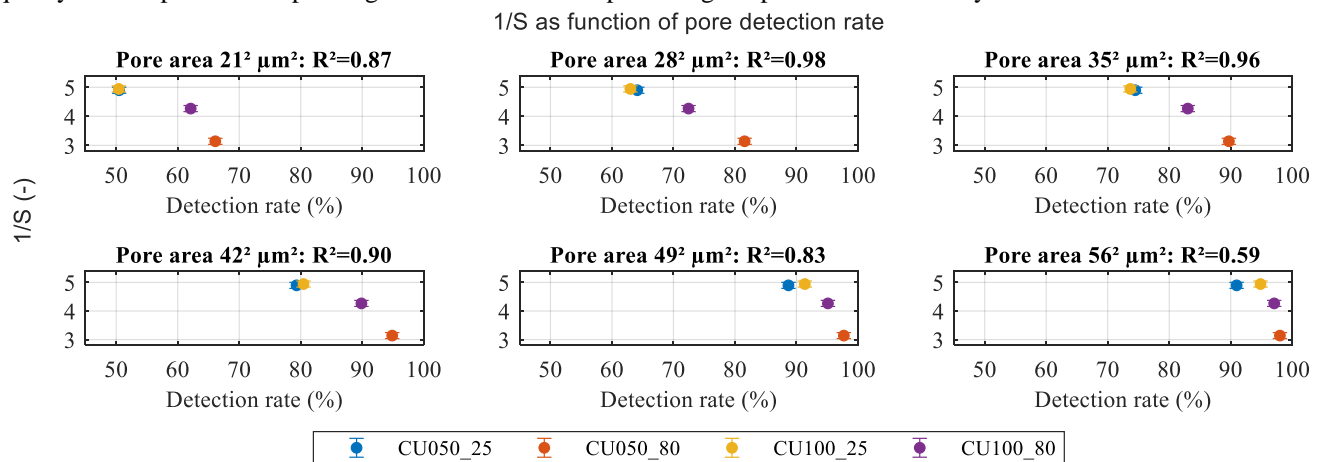


Figure 16: Influence of  $S$  on the pore detection rate for different minimal pore areas.

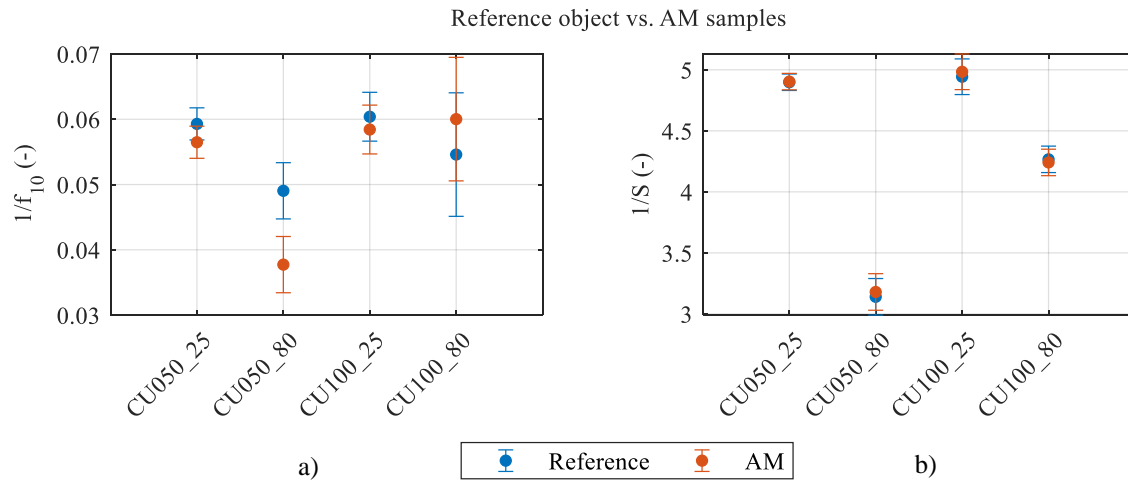


Figure 17: Comparison of  $f_{10}$  (a) and  $S$  (b) calculated using reference object and AM samples.

The parameter  $S$  describing image quality via sharpness at the part edges does not allow for a dimensional statement. However, it has several advantages. Compared to ISR, it does not include any surface determination step and is thus more representative for pore analysis tasks. Further, no complex and specifically designed reference object is required, as the evaluation can be carried out directly using the object edges. This work just evaluated cylindrical-shaped parts. Future research activities should focus on the transferability to more complex shaped parts to confirm the findings.

## 4 Summary and Conclusion

This work proposed a reference object (test object 1) for predicting the actual pore resolution in additively manufactured specimens (test object 2). Different performance parameters, assessable on the reference object, were evaluated and their transferability to real pore-containing AM samples was investigated. The reference object and the AM samples were scanned at four different "extreme" CT setting combinations for this purpose, then the resulting performance parameters and pore detection rate were correlated.

The ISR calculated by the point of contact of two touching spheres appeared appropriate for (quantitatively) predicting pore detection ability. However, obtaining a precise sphere contact point is not trivial. The  $f_{10}$ , deduced from the MTF, is a parameter that can be determined more easily. Yet,  $f_{10}$  was influenced by beam hardening and revealed little agreement between the reference object and actual AM specimens. As a generalization of  $f_{10}$ , the edge-based sharpness parameter  $S$  was investigated. This parameter appeared to be suitable for predicting pore detection rates as well as achieving transferable values from reference object to AM specimens. Using  $S$ , pore detection may be predicted even without a sophisticated reference object but directly on the real component. Therefore, it should be addressed in greater depth in future work. This is particularly relevant to the transferability to more complex component shapes as well as other materials or pore-inducing manufacturing processes. Additionally, the quantitative relationship between image quality and pore detection should be explored. In particular,  $S$ , unlike ISR, does not permit metric statements.

In general, it became apparent that pore analysis is a particularly complicated CT application field with considerable research potential. In addition to the pore size, pore shape is critical for pore detectability. Further research into a non-destructive approach for quantifying a CT system's pore detecting ability can yield several advantages. An appropriate parameter could aid in not only establishing good CT scanning parameters but also in defining feasible applications of the CT system on hand, in addition to enhancing the acceptance of CT systems as a measurement tool.

## Acknowledgements

The research documented in this manuscript/presentation has been funded by the Deutsche Forschungsgemeinschaft (DFG, German Research Foundation), project number 255730231, within the International Research Training Group "Integrated engineering of continuous-discontinuous long fiber reinforced polymer structures" (GRK 2078). The support by the German Research Foundation (DFG) is gratefully acknowledged.

## References

- [1] P. Hermanek, S. Carmignato, Porosity measurements by X-ray computed tomography: Accuracy evaluation using a calibrated object, *Precision Engineering* 49 (2017) 377–387. <https://doi.org/10.1016/j.precisioneng.2017.03.007>.
- [2] G. Kasperovich, J. Haubrich, J. Gussone, G. Requena, Correlation between porosity and processing parameters in TiAl6V4 produced by selective laser melting, *Materials & Design* 105 (2016) 160–170. <https://doi.org/10.1016/j.matdes.2016.05.070>.

- [3] W.W. Wits, S. Carmignato, F. Zanini, T.H. Vaneker, Porosity testing methods for the quality assessment of selective laser melted parts, *CIRP Annals* 65 (2016) 201–204. <https://doi.org/10.1016/j.cirp.2016.04.054>.
- [4] F. Léonard, S. Tamas-Williams, I. Todd, CT for Additive Manufacturing Process Characterisation: Assessment of melt strategies on defect population, in: *iCT 2016: 6th Conference on Industrial Computed Tomography*, 2016, pp. 1–8.
- [5] L. Schild, M. Fülling, B. Häfner, G. Lanza, Uncertainty Evaluation of Pore Analysis for Additively Manufactured Parts using Cross Sections, in: *9th Conference on Industrial Computed Tomography (iCT) 2019: Proceedings*, 2019.
- [6] J. Lifton, T. Liu, An adaptive thresholding algorithm for porosity measurement of additively manufactured metal test samples via X-ray computed tomography, *Additive Manufacturing* 39 (2021) 101899. <https://doi.org/10.1016/j.addma.2021.101899>.
- [7] Verein Deutscher Ingenieure, VDI/VDE 2630 Blatt 1.3: Computertomografie in der dimensionellen Messtechnik - Leitfaden zur Anwendung von DIN EN ISO 10360 für Koordinatenmessgeräte mit CT-Sensoren, Beuth Verlag GmbH, Berlin 17.040.30, 19.100, 35.240.80, 2011.
- [8] M. Bartscher, U. Neuschaefer-Rube, J. Illeemann, F. Borges de Oliveira, A. Stolfi, S. Carmignato, Qualification and Testing of CT Systems, in: S. Carmignato, W. Dewulf, R. Leach (Eds.), *Industrial X-ray computed tomography*, Springer, Cham, 2018, pp. 185–228.
- [9] E07 Committee, Test Method for Measurement of Computed Tomography (CT) System Performance, ASTM International 11.040.50, 2020.
- [10] W. Dewulf, H. Bosse, S. Carmignato, R. Leach, Advances in the metrological traceability and performance of X-ray computed tomography, *CIRP Annals* 71 (2022) 693–716. <https://doi.org/10.1016/j.cirp.2022.05.001>.
- [11] F. Zanini, S. Carmignato, Two-spheres method for evaluating the metrological structural resolution in dimensional computed tomography, *Meas. Sci. Technol.* 28 (2017) 114002. <https://doi.org/10.1088/1361-6501/aa85b7>.
- [12] Deutsches Institut für Normung e.V., Zerstörungsfreie Prüfung - Durchstrahlungsverfahren für Computertomographie - Teil\_3: Durchführung und Auswertung (ISO\_15708-3:2017); Deutsche Fassung EN\_ISO\_15708-3:2019, Beuth Verlag GmbH, Berlin 19.100, 2019.
- [13] K. Höger, L. Schild, G. Lanza, Influence of workpiece orientation for multimaterial measurements in dimensional computed tomography, in: *11th Conference on Industrial Computed Tomography (iCT) 2022: Proceedings*, 2022.
- [14] L. Schild, *Erzeugung und Verwendung von Anwendungswissen in der industriellen Computertomographie*, 1st ed., Shaker, Düren, 2022.